

# RSC Advances



This is an *Accepted Manuscript*, which has been through the Royal Society of Chemistry peer review process and has been accepted for publication.

*Accepted Manuscripts* are published online shortly after acceptance, before technical editing, formatting and proof reading. Using this free service, authors can make their results available to the community, in citable form, before we publish the edited article. This *Accepted Manuscript* will be replaced by the edited, formatted and paginated article as soon as this is available.

You can find more information about *Accepted Manuscripts* in the [Information for Authors](#).

Please note that technical editing may introduce minor changes to the text and/or graphics, which may alter content. The journal's standard [Terms & Conditions](#) and the [Ethical guidelines](#) still apply. In no event shall the Royal Society of Chemistry be held responsible for any errors or omissions in this *Accepted Manuscript* or any consequences arising from the use of any information it contains.

## A silica nanoparticle supported fluorescence “turn-on” fluoride ion sensing system with tunable structure and sensitivity

Richard Appiah-Ntiamoah<sup>1</sup>, Jadhav H. Arvind<sup>1</sup>, John. Marc. C. Puguan<sup>1</sup>, Francis W.Y. Momade<sup>2</sup>, Hern Kim<sup>1,\*</sup>

<sup>1</sup>*Department of Energy and Biotechnology, Energy and Environment Fusion Technology Center, Myongji University, Yongin, Kyonggi-do 449-728, Republic of Korea*

<sup>2</sup>*Department of Materials Engineering, Kwame Nkrumah University of Science and Technology (KNUST), Kumasi, Ghana*

\*Corresponding author: hernkim@mju.ac.kr, Tel: +82 31 330 6688; fax: +82 31 336 6336.

### Abstract

Amino-modified silica nanoparticles (*SNP-APTMS* and *SNP-TMSPEDA*), doped with silyl-ether protected fluorescein isothiocyanate (*FITC-OSMDBT*), were synthesized via a sol-gel method in an easy three-step reaction to give fluoride ion probes *SNP-TMSPEDA-FITC-OSMDBT* (sensor *A*) or *SNP-APTMS-FITC-OSMDBT* (sensor *B*). The as-prepared samples were characterized using FTIR, EDX, TGA, and fluorescence spectroscopy. The fluorescence intensity of both sensors increased when different concentrations of F<sup>-</sup> were added. It was found that, when the fluoride ion and *FITC-OSMDBT* mole equivalent titration ratio was  $x : x$ , the emission spectra for both sensors were the same only when  $x = 1.0$ ; At  $x = 3.0, 6.0,$  and  $9.0$ , sensor *B* displayed 3 folds the emission intensity of sensor *A*. This phenomenon was attributed to non-radiate emission energy transfer mechanisms, which are controlled by the *FITC-OSMDBT* loading density: the different degree of steric hindrance present on N-[3-(Trimethoxysilyl) propyl] ethylenediamine (TMSPEDA) and (3-aminopropyl)trimethoxysilane (APTMS) ensured that different amounts of *FITC-OSMDBT* were loaded on each sensor. Also, within this mole

equivalent titration ratio range, the emission intensity increased linearly with  $[F^-]$  in DMSO; thus, from the working curve of sensor **A**, the fluoride ion detection range of sensor **B** could be calculated and vice versa. The structure of the sensing system being proposed is simple, sensitive to  $F^-$ , and may prove useful with respect to the development fluoride anion sensors structures which can be easily modified to produce sensors with varying detection ranges.

**Keywords:** Fluoride ion; Fluoride sensor; Fluorescence; Detection range; Tunable- structure

## 1. Introduction

Fluoride ions, like many other anions, play a fundamental role in a wide range of chemical and biological process.<sup>1-4</sup> It has unique chemical properties and it is widely used in toothpaste and pharmaceutical agents for the prevention of dental caries, enamel demineralization while wearing orthodontic appliances, and treatment of osteoporosis.<sup>5</sup> Fluoride is also important in industrial applications and transformations, especially in steel making and aluminum refining, and it is a well established reagent in organic synthesis. Novel applications of fluoride have been discovered in the fields of ion batteries and in F-PET imaging. However, its benign health effect is up to 1ppm in living organisms, and it seems to be toxic at higher doses.<sup>6,7</sup> High concentration of fluoride in the environment and drinking water has been related to the occurrence of several types of pathologies in humans, such as osteoporosis, neurological and metabolic dysfunctions, and recently cancer.<sup>8</sup> This obvious health concerns have prompted scientists to develop analytical techniques which can accurately detect and quantify fluoride ions.

Among several widely used, fluoride-sensing and -detecting techniques, including the electrode method,<sup>9</sup> F NMR analysis,<sup>10</sup> and colorimetric (UV) and fluorescence sensing, electrochemical systems are the most well-established. However, this approach has major disadvantages associated with the need for fragile instrumentation and time-consuming manipulations.<sup>11</sup> In addition; F NMR spectroscopy can be used reliably to detect only micromolar levels of fluoride. Moreover, neither the electrochemical nor the NMR approach can be miniaturized for use in studying biological processes in vivo.<sup>12</sup> To this end, other detection techniques, particularly those that are based on fluorescence and color change, have been intensely studied; and so far, they have shown to have great promise considering their high selectivity, sensitivity, response time, and ease of use in both intra- and extra-cellular environments. These types of sensor usually consist of three moieties: fluorophore/chemophore, spacer and receptor. Their optical signal changes upon binding of F<sup>-</sup> and their common adopted sensing strategy involves supramolecular interactions such as anion- $\pi$  interactions, hydrogen bonding and Lewis acid/base interactions.<sup>13-16</sup> Several fluorescent fluoride chemosensors and chemodosimeters works have been developed and reported in literature.<sup>17-23</sup> Fluorescence chemodosimeters are reaction-based: they utilize F<sup>-</sup> promoted cleavage reactions and hence, they are more selective towards F<sup>-</sup> than chemosensors;<sup>12</sup> besides, they work better in organic and/or aqueous solutions.<sup>24</sup> Thus, they are preferred to fluorescence chemosensors.

In the mean time, scientist have focused on developing ultra sensitivity and selective, and highly responsive fluorescent fluoride chemodosimeters using mainly organic materials to detect fluoride ions in organic media.<sup>18-22</sup> But with the challenge of sensing F<sup>-</sup> in organic media seemingly solved, attention has now been focused to sensing F<sup>-</sup> in aqueous media. Recent reports show that a lot of progress has been made in this field as well with some reporting fluoride

fluorescent chemodosimeters with amazing sensitivity, selectivity, and response time values.<sup>24,25</sup> Another area that has received a lot of attention is the use of organic-inorganic materials to recognize and sense fluoride. Receptors immobilized on inorganic materials such as SiO<sub>2</sub>, Al<sub>2</sub>O<sub>3</sub>, and TiO<sub>2</sub> have many advantages such as Organic-inorganic hybrids nanomaterials can be recycled through suitable chemical treatment, and functionalized nanomaterials combined with fluorophores display highly selective and sensitive fluorescence or absorption changes because of their large surface area and well-defined pores.<sup>12</sup> A few examples of such F<sup>-</sup> detection systems exist in literature: a method of detecting fluoride in water based on the specific reaction of fluorhydric acid with an MCM-41 solid functionalized with fluorescent or colorimetric signaling unit has been reported.<sup>26</sup> Furthermore, a novel covalently bonded luminescent hybrid material and its spectrophotometric anion-sensing properties were described in literature.<sup>27</sup>

Despite the advances in fluorescent fluoride sensor development, the fact that most of these sensors are developed to be a 'one-solution-fit-all' kind of material, with the best sensitivity, selectivity, and response time, makes their use both good and bad: For example, drinking-water regulatory bodies (e.g. EPA) need highly selective and sensitive F<sup>-</sup> sensor with a narrow detection range since they only have to check if the concentration of F<sup>-</sup> is below or above 2 ppm; However, for laboratory reactions and industrial applications (e.g. steel-making, batteries, and toothpaste manufacturing), higher concentrations of fluoride are used, and hence, a sensor with a wider detection range is preferred. It therefore seems economically unwise to focus on developing only ultra sensitive and selective sensors which on the average is bound to be expensive. To the best of our knowledge, no work has been done to investigate the use of an organic-inorganic fluorescence turn-on F<sup>-</sup> sensing system having a structure which can be easily modified to vary its detection range. Most of the chemodosimeters reported in literature makes

use of organic fluorescent dyes to transduce the chemical interactions between  $F^-$  and the sensor into optical signals which are recorded by UV-vis- and/or fluoro-spectrophotometer. The spectra change of the dye serves as the basis on which its sensitivity and selectivity, and response time are evaluated.

Herein, silyl-ether protected fluorescein isothiocyanate (*FITC-OSMDBT*) molecules were covalently immobilized on silica nanoparticles (SNP) surfaces separately functionalized with two different amino-molecules to form sensors *A* and *B*. The effect of *FITC-OSMDBT* percentage (%) loading on the emission spectra of each sensor in the presence of  $F^-$  was investigated separately, and after which the two results were correlated to show the relationship between their emission intensity increments and their detection ranges. Using this correlation, we hope to show that, by carefully controlling the *FITC-OSMDBT* loading amount, with different coupling agents, the sensitivity of the sensor may be varied extensively. The selectivity and response time of both sensors in the presence of  $Cl^-$ ,  $Br^-$ ,  $I^-$ , and  $NO_3^-$  were also determined and compared with that of  $F^-$ .

## 2. Experimental

### 2.1. Materials

Silicon dioxide nanoparticles (SNP) from Sigma-Aldrich with a particle size range of 10.0 – 20.0 nm were used for this experiment. 3-aminopropyltrimethoxysilane (APTMS) and N-[3-(Trimethoxysilyl)propyl]ethylenediamine (both from Sigma-Aldrich, 97.0%) were used to modify the SNP and graft Fluorescein 5(6) Isothiocyanate (FITC) molecules (Sigma-Aldrich,  $\geq$

90.0%). The chemical structures of the amino-molecules are illustrated in Table 1. The other chemicals used included triple distilled water, anhydrous acetonitrile (99.8%), anhydrous toluene (Acros, 99.8%), anhydrous DMSO (Fisher, 99.9%), anhydrous DCM (Acros, 99.8%), absolute ethanol (Merck KGaA, 99.5%), tetrabutylammonium fluoride hydrate (98%), tetrabutylammonium nitrate (97%), tetrabutylammonium iodide (98.0%), tetrabutylammonium chloride hydrate (98.0%), tetrabutylammonium bromide ( $\geq 98.0\%$ ), triethylamine ( $\geq 99.0\%$ ), and tert-Butyldimethylsilylchloride (TBDMSCl), ( $\geq 97.0\%$ ) (all from Sigma-Aldrich). Unless otherwise stated, all the chemicals used were of analytical grade and were used as received without further purification.

## 2.2. Characterization

Transmittance infrared spectra of the various attached functional groups were collected using a Varian FTS 2000 Fourier Transform Infrared (FT-IR) spectrometer. The weight change after each synthesis step was analyzed via TGA measurements using Perkin-Elmer TGA-7 instrument, a standard platinum crucibles and a sample size of 20.0 mg were used. The samples were heated at a rate of 10.0°C min from room temperature to 1000.0°C in an N<sub>2</sub> flow of 50.0 ml min<sup>-1</sup>. Elemental composition analysis was done with Dispersive X-Ray spectrometry (EDX) with a scanning electron electrode at 20 kV. Lastly, surface area and the pore diameter changes were measure via BET and BJH analysis.

The anion solution (all anions as tetrabutylammonium (TBA) salts, 0.1-9.0 equiv. with respect to the amount of *FITC-OSMDBT* anchored on SNP) was titrated against different concentrations of sensors *A* and *B* and mixed for 5.0 min. Their absorption and emission changes

were then measured using Cary 100 UV-Visible spectrophotometer and Hitachi F-4600 fluorescence spectrometer respectively.

## 2.3. Synthesis of silica nanoparticle supported fluorescence turn-on sensor

### 2.3.1. Silylation of SNP with amino-functional trimethoxysilanes

The silylation method used was essentially similar to that reported in literature,<sup>27</sup> except that, the ratio of SNP to TMSPEDA (or APTMS) was changed. Briefly, 0.2 g of SNP was mixed with 30.0 ml of TMSPEDA (or APTMS) solution (2.0% v/v in toluene) and agitated under reflux at 110.0°C for 24.0 h in N<sub>2</sub> atmosphere. The modified silica nanoparticles were isolated and purified by centrifugation/redispersion processes in toluene (for 30.0 min at 16,000 rpm, 6 times) to remove unreacted and loosely bound TMSPEDA (or APTMS). Finally, the purified solid was cured at 110.0°C for 12.0 h in a conventional oven after which it cooled in a desiccator. ***SNP-TMSPEDA*** (or ***SNP-APTMS***) was used to denote the cured solid.

### 2.3.2. Immobilization of FITC on silanized SNP

0.5g of ***SNP-TMSPEDA*** (or ***SNP-APTMS***) was dissolved in 30.0 ml of absolute ethanol and stirred for 10.0 min, after which a calculated amount of FITC [1.5 fold excess relative to the amount of grafted TMSPEDA (or APTMS)] was added to the suspension. The resulting mixture was stirred for 24.0 h in the dark at room temperature. Then, the red product was collected and washed (for 20.0 min at 16,000 rpm, 4 times) copiously with absolute ethanol until the filtrate was clear of color. Finally, the purified solid was oven dried at 80.0°C for 1h and was denoted as ***SNP-TMSPEDA-FITC*** (or ***SNP-APTMS-FITC***).



### 2.3.3. Silylation of phenol groups on FITC with TBDMSCl

A mixture of *SNP-TMSPEDA-FITC* (or *SNP-APTMS-FITC*) (0.2 g), anhydrous DCM (10.0 ml), and triethylamine (78.0 mg) in a beaker was stirred under nitrogen atmosphere for 30.0 min while the beaker was immersed in a mixture of cracked ice and water. 0.6 mg of TBDMSCl in 5.0 ml DCM was added drop-wise into the reaction mixture after which it was stirred for an additional 18.0 h. Then, the light yellow product was filtered and washed several times with acetonitrile and water. The purified sample was then dried under vacuum for 48.0 h at room temperature. The final product was denoted as *SNP-TMSPEDA-SFITC-OSMDBT* (sensor *A*) [or *SNP-APTMS-FITC-OSMDBT* (sensor *B*)]

## 3. Results and discussion

### 3.1. Surface group analysis

Sensors *A* and *B* possessing FITC and Si-O as fluorescent unit and fluoride sensing site respectively were synthesized as shown in Scheme 1. FT-IR analysis was used to follow the synthesis reaction of each sensor. In both cases, certain relevant peaks were identified and used to verify each reaction step. Fig. 1 shows the peaks of sensors *A* and *B* as well as that of their intermediate products. After the silanization reaction, the silanol peak at  $\sim 956.0\text{ cm}^{-1}$  on SNP vanished, while peaks belonging to  $-\text{CH}_2$  ( $\sim 2924.0\text{ cm}^{-1}$ ) and  $-\text{NH}_2$  ( $\sim 1543.0\text{ cm}^{-1}$ ) groups appeared.<sup>27</sup> This confirmed the condensation reaction between the silanol groups and alkoxy silanes. The N-H stretching peaks for both APTMS and TMSPEDA was overshadowed by the much broader and intense -OH peak at  $\sim 3500.0\text{ cm}^{-1}$ , the sharp and strong Si-O-Si stretching peak at  $\sim 1080.0\text{ cm}^{-1}$  was observed in all the samples, which indicated that the main structure of SNP did not change.

New peaks could be seen after the FITC immobilization reaction: the peaks from  $\sim 1620.0$   $\text{cm}^{-1}$  to  $\sim 1303.0$   $\text{cm}^{-1}$  belong to the aromatic rings of FITC, while that from  $\sim 914.0$   $\text{cm}^{-1}$  to  $\sim 902.0$   $\text{cm}^{-1}$  belong to the aromatic  $-\text{CH}$  bending vibrations.<sup>28</sup> The lactone peak was overshadowed by the benzene ring peaks. Likewise, the thione ( $-\text{C}=\text{S}$ ) peak was masked by the much dominant Si-O-Si peak. The C-H stretching vibrations at  $\sim 2939.0$   $\text{cm}^{-1}$  became more prominent after the silylation reaction which indicates the presence of  $\text{CH}_3$  groups belonging to the TBDMSCl. In like manner, the Si-O-Si stretching peak at  $\sim 1080.0$   $\text{cm}^{-1}$  also increased in intensity. Furthermore, strong fluorescence was not observed when solutions of both sensors were irradiated with 520.0 nm light, which suggested that *FITC-OSMDBT* had been successfully protected. Base on these results, it was assumed that the moieties were covalently bonded to SNP.

EDX analysis showed weight % and atomic % of various elements (C, O, Si and S) in sensors *A*, and *B*; but, only elements O and Si were present in SNP (Table 2), which further confirms that the modification reaction was successful. Furthermore, the weight % and atomic % of elements C, Si, and S varied strongly among the sensors: sensor *A* had a higher weight % and atomic % of Si and S than sensor *B*, while sensor *B* has a higher C content. A higher S value means that, sensor *A* has higher FITC loading on its surface, and thus more *FITC-OSMDBT* molecules as indicated by its high Si value. While the higher C content in sensor *B* reflects its TMSPEDA content.

The effect of surface modification on the surface area and pore diameter of SNP, sensor *A*, and sensor *B* were studied via nitrogen adsorption-desorption isotherms and Barrett-Joyner-Halenda (BJH) pore diameters analysis as shown in Fig. 2. Results from Fig. 2 (shown in table 3) revealed that, before modification, SNP had a Brunauer-Emmett-Teller (BET) surface area of  $674.65$   $\text{m}^2$   $\text{g}^{-1}$  and a pore volume of  $0.77$   $\text{cm}^3$   $\text{g}^{-1}$ . In contrast, sensors *A* and *B* had lower BET

surface areas (98.81 161.05 and 161.05 m<sup>2</sup> g<sup>-1</sup>, respectively) and pore-volume (0.18 and 0.24 cm<sup>3</sup> g<sup>-1</sup>, respectively). The BJH pore diameter was narrow for all the samples: 4.58 nm for SNP, and 5.97 and 7.19 nm for sensors *A* and *B* respectively. The smaller surface area and pore diameter of the sensors compared to SNP suggest that the modification reaction was successful, and also the higher surface loading of sensor *A* compared to sensor *B*.

### 3.2. Determination of *FITC-OSMDBT* loading density via TGA

Theoretically, the amount of *FITC-OSMDBT* immobilized on each sensor should determine the concentration of F<sup>-</sup> it can detect, since it is this part of the sensor which reacts with F<sup>-</sup> to induce fluorescence change. The amount of *FITC-OSMDBT* per gram of each sensor was determined using the weight loss due to TBDMSCI calculated using TGA analysis. The thermogram of sensor *A* (Fig. 3) indicates that, the pure SNP lost moisture and underwent dehydroxylation in a single step process between 120.0°C and 1000.0°C, just as reported in literature,<sup>29</sup> with an accompanying weight loss of about 4.14%. For the *SNP-APTMS* material, it first suffered a loss of about 5.84% due to moisture and then, as expected, decomposed in two steps: the first loss of about 8.24% (associated with the loss of APTMS) occurred between 120.0°C and 470.0°C, while the second loss was about 5.17% (associated with the loss of intraglobular hydroxyl groups) occurred between 470.0°C and 1000.0°C. It has been reported that temperatures above 650.0°C are required to remove all intraglobular hydroxyl groups,<sup>30</sup> hence, it was assumed that all losses above 650.0°C is due only to dehydroxylation. For the *SNP-APTMS-FITC* sample, the weight loss due to moisture was about 3.94% after which it decomposed, as expected, in three steps: the first weight loss of about 1.79% occurred between 100.0°C and 230.0°C, the second ~8.44% occurred between 230.0°C and 450.0°C, and the third

~10.89% occurred between 450.0°C and 1000.0°C. The first loss was attributed to APTMS because it has a lower boiling point than FITC (92.0°C and 400.0°C respectively). Lastly, the *SNP-APTMS-FITC-OSMDBT* material also suffered an initial loss of 4.14% due to moisture; but, it decomposed in only two steps afterward instead of the expected four. The first was between 120.0°C and 630.0°C, and the second was between 630.0°C and 1000.0°C. The weight loss at this first temperature range was 20.22%, which is higher than the 10.22% (1.79% + 8.44%) loss recorded for APTMS and FITC in sample *SNP-APTMS-FITC*. Assuming that no leaching occurred during the heating process, the *OSMDBT* amount was estimated as 10.00% (20.22% - 10.22%); hence, the *FITC-OSMDBT* amount was 0.66mmol/g.

The thermogram of sensor *B* and its intermediate products suggest that the organic moieties on sensor *B* undergo similar degradation steps as those on sensor *A*, except for the difference in amount of weight loss. The SNP is seen to undergo the same two-step decomposition process: the first due to moisture loss and the second due to dehydroxylation. Similarly, the *SNP-TMSPEDA* material decomposed in a two-step reaction after the initial moisture loss. The loss due to TMSPEDA (which occurred between 130.0°C and 450.0°C) was 13.29% compared to the 8.24% recorded for APTMS. This was expected since TMSPEDA is bulkier than APTMS. However, the FITC amount on *SNP-TMSPEDA-FITC* was lower than that on *SNP-APTMS-FITC*: The mole per gram was 0.058 : 0.084 respectively. This suggests that the weight of immobilized TMSPEDA was higher than that of APTMS; but, the APTMS molecules were greater in number than TMSPEDA. Lastly, *SNP-TMSPEDA-FITC-OSMDBT* also underwent two decomposition steps after its initial moisture loss of 3.28%. The amount of *OSMDBT* immobilized was calculated to be 7.40%; hence, the *FITC-OSMDBT* amount was 0.49mmol/g. Table 4 puts the results into perspective.

### 3.3. Absorbance change and Fluorescence turn-on sensing for $F^-$ in DMSO

The TGA results clearly indicate that sensor **A** has higher **FITC-OSMDBT** loading than sensor **B**. Next up, we investigated how these varying **FITC-OSMDBT** loading amounts affected the emission and absorption spectra of each sensor in the presence of different amounts of  $F^-$ . The ‘effect’ on each sensor for a given  $[F^-]$  was quantified in terms of emission intensity change and compared to find any useful correlation between them. This correlation was then related to the  $[F^-]$  to find the detection range of each sensor.

To begin with, low concentrations of  $F^-$  (0.0 to 1.0 mole equiv.) were titrated against each sensor solution containing 1.0 mole equiv. of **FITC-OSMDBT** in DMSO. The resulting fluorescence spectra (Fig. 4) and absorbance spectra (Fig. 5) show that both sensors clearly exhibited very weak absorption and emission in the absence of  $F^-$ ; however, with the addition of the fluoride anion, the absorbance and fluorescence intensity of both sensors gradually increased, and then leveled off when  $[F^-]$  reached 50.0 mM (1.0 mole equiv.  $F^-$ ). The fluorescence ‘turn-on’ indicated the successful reaction between  $F^-$  and Si-O. Working curves established by plotting the increase in emission intensity at 542 nm vs.  $[F^-]$  (insert of Fig. 5b) indicate that, the emission intensity increment for both sensors were nearly the same at every  $[F^-]$ . Which suggested that at low  $[F^-]$ , the emission spectra of sensor **A** and **B** are independent of **FITC-OSMDBT** loading amount. Also, the emission intensity increment for both sensors varied linearly with  $[F^-]$  between 10.0 mM to 40.0 mM (insert of Fig. 5a); thus, this concentration range was chosen to be the detection range of both sensors. However, an interesting emission spectra pattern was observed when 3.0 mole equiv.  $F^-$  was titrated against three solutions of each sensor containing 3.0, 6.0 and 9.0 mole equiv. of **FITC-OSMDBT** as depicted in scheme 2.

For sensor **A**, all 3 titrations produced different emission intensity values which increased consecutively in the order of: **n**, **2n**, and **3n** for the 3.0, 6.0, and 9.0 mole equiv. respectively as shown in the insert of schematic 2. We therefore assumed that, for every 3 mole equiv. **FITC-OSMDBT** available for  $F^-$  detection, only one reacted with 1.0 mole equiv.  $F^-$  and showed emission intensity corresponding to 1.0 mole equiv.  $F^-$ . The fact that the value of **n** (54983.85 a.u.) was approximately equal to that produced by 1.0 : 1.0 mole equivalent titration between fluoride ion and SFITC (54189.50 a.u.) meant that the above assumption might be true. Besides, the emission intensity increment varied linearly with  $[F^-]$  in all three titration, a fact which also supported the assumption. Based on this linear relationship, the detection range for the 3.0, 6.0, and 9.0 mole equiv. **FITC-OSMDBT** solutions were calculated as to be: 0.0 ~ 50.0 mM, 0.0 ~ 100.0 mM, and 0.0 ~ 150.0 mM respectively.

Sensor **B**, on the other hand, produced approximately the same emission intensity value (**m**) for all three titrations (insert of schematic 2), and this value was approximately equal to **3n**. Unlike sensor **A**, this observation meant that all 3.0 mole equiv. **FITC-OSMDBT** were able to detect all 3.0 mole equiv. of  $F^-$ ; and thus, the detection range of sensor **B** was assumed  $\approx$  3.0 folds that of sensor **A** for solutions of both sensors containing the same equiv. amount of **FITC-OSMDBT**. The close correlation between **3n** and **m** corroborates the earlier assumption we made relating  $[F^-]$  and intensity in sensor **A**. The detection range of sensor **B** was calculated to be 0.0 ~ 150.0 mM for all three titrations.

To further test the validity of our assumption, the above experiment was repeated by titrating 3.0, 6.0, and 9.0 mole equiv.  $F^-$  solutions against their corresponding sensor solutions containing 3.0, 6.0, and 9.0 mole equiv. **FITC-OSMDBT** respectively; their emission spectra (insert of Fig. 6a) clearly shows the big difference in emission intensity between the sensors: To our surprise,

Sensor **A** gave emission intensity values in the order of: **n**, **2n**, and **3n** respectively: just like before. However, the emission values of sensor **B** increased in the order **m**, **2m**, and **3m** respectively as shown in the Fig. 6a. A comparison between the emission values revealed that, **m**  $\approx$  **3n**, **2m**  $\approx$  **6n**, and **3m**  $\approx$  **9n**: A result which confirms our earlier assumption. We could therefore conclude that for a given solution of sensor **A** and sensor **B** containing equimolar amounts of *FITC-OSMDBT*, the  $F^-$  detection limit of sensor **B** is thrice (3X) that of sensor **A**. Also, the emission intensity values of **m**, **2m**, and **3m** varied linearly with their corresponding  $[F^-]$ . The detection range of sensor **B** was predicted from the working curve constructed for sensor **A**, shown in the insert of Fig. 6b. From this curve, the  $F^-$  detection range values were calculated as follows: For sensor **A**; 0.0 ~ 50.0 mM, 0.0 ~ 100.0 mM, and 0.0 ~ 150.0 mM respectively; and sensor **B**; 0.0 ~ 150.0 mM, 0.0 ~ 300.0 mM, and 0.0 ~ 450.0 mM respectively. A repeat of the experiment with other mole equiv. titration ratios  $x : x$  ( $x = 2.0, 4.0, \text{ and } 5.0$ ) of  $F^-$  and *FITC-OSMDBT* failed to give emission intensity values which could correlate the concentration and detection range of both sensors. Fig. 7a shows how erratic the emission intensity values for both sensors changed with concentration.

In literature, a well known mechanism reported for  $F^-$  sensing with similar sensors involves an irreversible reaction between  $F^-$  and the Si-O bond of the sensors which generates a transducing fluorophore.<sup>24,25,33</sup> Our sensor showed a similar pattern, so it was assumed that a similar reaction took place (as shown in Fig. S1). This mechanism is, nonetheless, insufficient to explain the unusual pattern observed in sensors **A** and **B**. Besides, the TGA results indicated that sensor **A** has a higher percentage loading of *FITC-OSMDBT* than sensor **B**, hence as reported in literature,<sup>31</sup> the former should exhibit greater fluorescence intensity than the latter; but, it did not.

A detailed study focused on the orientation, size, and distance dependence of energy transfer mechanisms amongst the conjugated parts of the receptor before and after its reaction with fluoride anions is necessary to uncover the complete picture. We are currently working on another paper which may aid us in this direction. With that said, we made the following assumptions regarding the probable underlying mechanism based on the results obtained in our studies and some reported results in literature.

The absorption and emission spectrum of as-prepared *SNP-TMSPEDA-FITC* was studied with and without fluoride anions. The spectra obtained (as shown in Fig. S2) were identical, clearly indicating that  $F^-$  did not have any influence on the spectra of *SNP-TMSPEDA-FITC*. The result was however different for *SNP-TMSPEDA-FITC<sup>a</sup>* generated after *SNP-TMSPEDA-FITC-OSMDBT* titration with fluoride ions (shown in Fig. S1). As shown in Fig. S2, the absorption and fluorescence spectra of *SNP-TMSPEDA-FITC<sup>a</sup>* showed a bathochromic shift and reduced intensity.

The bathochromic shift and reduced intensity may be explained by considering the entities present in the titration solution. As noted earlier,  $F^-$  has no effect on the spectrum of *SNP-TMSPEDA-FITC* and by extension on that of *SNP-TMSPEDA-FITC<sup>a</sup>* as well; however, it appears unreacted *SNP-TMSPEDA-FITC-OSMDBT* molecules do. The FT-IR spectra of *TMSPEDA-FITC<sup>a</sup>* and as-prepared *SNP-TMSPEDA-FITC-OSMDBT* (shown in Fig. S3) appear to be similar which suggest the presence of unreacted *SNP-TMSPEDA-FITC-OSMDBT* molecules on the receptor even after the cleavage reaction with  $F^-$ . An example of changes in the lifetime of dye molecules as well as the rate of their nonradiative energy transfer while in the vicinity of other entities it interacts with have been reported in literature.<sup>32</sup> Perhaps, the “new” emission spectrum of *SNP-TMSPEDA-FITC<sup>a</sup>* overlapped with the absorption spectrum of the



conjugated segment in unreacted *SNP-TMSPEDA-FITC-OSMDBT* or vice versa to cause non-radiative emission energy transfer (nEET) interactions between the two species. Hence, the observed reduction in fluorescence intensity and bathochromic shift.

Furthermore, nEET is known to be governed by coulombic or/and dipole interactions.<sup>32</sup> In DMSO, *SNP-TMSPEDA-FITC<sup>a</sup>* is dianionic,<sup>25</sup> and Si-O bonds are reported to have a dipole moment.<sup>34</sup> These two factors could have therefore induced energy transfer interactions between the two entities and lead to nEET.

With a higher density of *SNP-TMSPEDA-FITC-OSMDBT* molecules, sensor *A* is likely to have more unreacted *SNP-TMSPEDA-FITC-OSMDBT* than sensor *B*. Also, the closer proximity of its *SNP-TMSPEDA-FITC-OSMDBT* molecules, as indicated by the TGA data, makes sensor *A* more prone to higher rates of nEET according to Equation (1)<sup>32</sup> because if it smaller *R* value. This might explain why sensor *A* exhibited weaker fluorescence intensity, despite having more *FITC-OSMDBT* molecules.

$$k_{DA} = k_{rad} \left( \frac{R_F}{R} \right)^6 \quad (1)$$

where:

$k_{DA}$  is the non-radiative energy transfer

$k_{rad}$  is the radiative rate,

*R* the center to center separation distance between the silyl-protected receptor 1 molecules

$R_F$  is the Forster radius

### 3.4. Response time and selectivity performance of the sensing systems

The response time of sensor **A** and sensor **B** towards  $F^-$  was investigated by measuring their emission increment with time after the addition of  $F^-$ . The results, as shown in Fig. 7b, indicated that the reaction between the sensors and the fluoride anions reached equilibrium quite fast ( $\sim 4$ min), which suggested that both sensors were well dispersed in solution, and thus, allowed the Si-O active sites to be readily accessed by fluoride anions. The results prove that both sensors are highly responsive toward fluoride anions.

The next property of the sensors was investigated using their selectivity towards  $F^-$  over other anions. The emission spectra of sensors **A** and **B** in the presence of other anions including  $Cl^-$ ,  $Br^-$ ,  $I^-$ , and  $NO_3^-$  were recorded and the results compared to that of  $F^-$ . From the results shown in Fig. 8, it is clear that only  $F^-$  induced the most prominent emission intensity change, whereas, the addition of other anions under the same conditions led to almost no change in emission intensity. At 1.0 : 1.0 ( $F^-$  : **FITC-OSMDBT**) equiv. mole titration ratio, the selective of the two sensors was almost the same (Fig. 8a); A pattern which is similar to that observed with their detection limit value. However, at 3.0 : 3.0 equiv. mole titration ratio, sensor **B** showed better results than sensor **A** (Fig. 7b): its intensity value was 2.6 folds that of sensor **A**. Nonetheless, the results show that both sensors exhibit good selectivity towards  $F^-$  over other anions, a feature which was attributed to the affinity of  $F^-$  for Si-O.<sup>25</sup> The bright yellow color of given off by sensor **B** solution in the presence of  $F^-$  under a hand-held UV lamp, as shown in Fig. 9, shows the highly selectivity nature of the sensor. Table 5 puts the performance of the two sensors into perspective.

## 4. Conclusions

We have successfully synthesized an easy to make fluorescence turn-on highly responsive, and selective silica nanoparticle (SNP) supported  $F^-$  sensing system having a structure which can be easily modified to vary its sensitivity towards  $F^-$  in DMSO. FTIR, TGA, EDX, fluorescence spectroscopy analysis data were used to show the successful synthesis of the sensing system. In this paper, APTMS and TMSPEDA modified SNP were used to show two variations of the sensing system structure and their sensing properties. The amino-molecules helped to vary the percentage (%) loading of silyl-ether protected fluorescein isothiocyanate (*FITC-OSMDBT*) on each sensor, which in turn, helped to regulate the emission spectra of each sensor through non-radiative emission energy transfer (nEET) mechanisms. At 1.0 : 1.0 ( $F^-$  : *FITC-OSMDBT*) equiv. mole titration ratio, the emission intensity and detection range values of both sensors were the same; however, at equiv. mole titration ratio  $x : x$  ( $x = 3.0, 6.0, \text{ and } 9.0$ ), the emission intensity increment in sensor **B** was found to be thrice that of sensor **A**. A linear correlation was established between the emission intensity values and detection range of both sensors. From this linear correlation, the detection limit of sensor **B** was found to be thrice that of sensor **A**. Finally, at  $x : x$  ( $x = 2.0, 4.0, \text{ and } 5.0$ ) molar titration ratio, no correlation could be made between the emission increment with concentration. The reason why this phenomenon was peculiar to  $x : x$  ( $x = 3.0, 6.0, \text{ and } 9.0$ ) molar titration ratios appears to be due to non-radiative emission energy transfer mechanisms; the details of this underlining phenomenon is under investigation. Nonetheless, the current results prove that this type of sensor architecture may prove useful for the development of  $F^-$  sensing systems with specific detection limits.

## Acknowledgement

This research work was supported by the National Research Foundation of Korea NRF-Grants funded by the Ministry of Science, ICT and Future Planning \_2001-003090) and the Ministry of Education (2009-009816), Republic of Korea.

## References

1. R. M. Duke, E. B. Veale, F. M. Pfeffer, P. E. Kuger and T. Gunnlaugs-son, *Chem. Soc. Rev.* 2010, **39**, 3936-3953.
2. E. Galbraith and T. D. Jams, *Chem. Soc. Rev.* 2010, **39**, 3831-3842.
3. R. Martinez-Manez and F. Sancenon, *Chem. Rev.* 2003, **103**, 4419-1776.
4. A. N. Swinburne, M. J. Paterson, A. Beeby and J. W. Steed, *Chem. Eur. J.* 2010, **16**, 2714-2718.
5. C. R. Wade, A. J. Broomsgrove, S. Aldridge and F. P. Gabbai, *Chem. Rev.* 2010, **110**, 3958-3984.
6. S. Jagtap, M.K. Yenkie, N. Labhsetwar, S. Rayalu, *Chem. Rev.* 2012, **112**, 2454-2466.
7. R. Wu, S. S. Qian, F. Hao, H. Cheng, D. Zhu and J. Zhang, *Environ. Sci. Technol.* 2011, **45**, 6041-6048.
8. C. Costamagna, A. Bosia and D. Ghigo, *Crr. Med. Chem.* 2010, **17**, 2431-2441.
9. P. Cosentino, B. Grossman, C. Shiek, S. Doi, H. Xi and P. Erbland, *J. Geotech. Eng.* 1995, **121**, 610-617.
10. P. Konieczka and B. Namiesnik, *J. Bul. Environ. Contam. Toxicol.* 200, **64**, 794-803.
11. K. Itai and H. Tsunoda, *Clin. Chim. Acta*, 2001, **308**, 163-171.
12. Z. Ying and Z. F. Jun, Y. Juyoung, *Chem. Rev.* 2014, **114**, 5511-5571.
13. Z. Xu, S. K. Kim, S. J. Han, C. Lee, G. Kociok-Kohn, T. D. James and J. Yoon, *Eur. J.*

- Org. Chem.* 2009, 18, 3058-3065.
14. Z. Q. Lui, M. Shi, F. Y. Li, Q. Fang, Z. H. Chen, T. Yi and C. H. Huang, *Org. Lett.* 2005, 7, 5481-5484.
15. X. Y. Lui, D. R. Bai and S. N. Wang, *Angew. Chem.* 2006, **118**, 5601-5604.
16. Y. Kubo, M. Yamamoto, M. Ikeda, M. Takeuchi, S. Shinkai, S. Yamaguchi, K. Tamao, *Angew. Chem. Int. Ed.* 2003, **42**, 2036-2040.
17. W. C. Anthony, *Fluorescent Chemosensors for Ion and Molecule Recognition*, Vol. 538, American Chemical Society, 1993.
18. T. -H. Kim and T. M. Swager, *Angew. Chem. Int. Ed.* 2003, **42**, 4803-4806.
19. Y. Kubo, M. Yamamoto, M. Ikeda, M. Takeuchi, S. Shinkai, S. Yamaguchi and K. Tamao, *Angew. Chem. Int. Ed.* 2003, **42**, 2036-2040.
20. Q. -Y. Chen and C. -F. Chen, *Tetrahedron Lett.* 2004, **45**, 6493-6496.
21. S. J. M. Koskela, T. M. Fyles and T. D. James, *Chem. Commun.* 2005, 7, 945-947.
22. Y. Kubo, T. Ishida, A. Kobayashi and T.D. James, *J. Mater. Chem.* 2005, **15**, 2889-2895.
23. S. Y. Kim and J. -I. Hong, *Org. Lett.* 2007, **9**, 3109-3112.
24. P. Sokkalingam and C. -H. Lee, *J. Org. Chem.* 2011, **76**, 3820-3828.
25. F. Zheng, F. Zeng, C. Yu, X. Hou and S. Wu, *Chem. Eur. J.* 2013, 19, 936-942.
26. A.B. Descalzo, D. Jimenez, J.E. Haskouri, D. Beltran, P. Amoros, M.D. Marcos, R. Martinez-Manez and J. Soto, *J. Chem. Commun.* 2002, **6**, 562-563.
27. P. Vejayakumaran, I. A. Rahmana, C.S. Sipaut, J. Ismail and C.K. Chee, *J. Colloid Interface Sci.* 2008, **1**, 81-91.
28. G. Feng, L. Fabao, Y. Jun and W. Lun, *Luminescence*, 2008, **23**, 392-396.
29. E. Satu, A. Root, M. Peussa and L. Niinisto, *Thermochemica acta*, 2001, **379**, 201-212.

30. E. F. Vasant, P. Van Der Voort, K. C. Vrancken, Characterization and chemical modification of silica surface, Elsevier, Amsterdam, 1995 (chapters 1-6).
31. E. Kim, H. J. Kim, D. R. Bae, S. J. Lee, E. J. Cho, M. R. Seo, J. S. Kim and J. H. Jung, *New J. Chem.*, 2008, **32**, 1003–1007.
32. S. Saini, S. Bhowmick, V. B. Shenoy and B. Bagchi, *J. Photochem. Photobio. A*, 2007, **190**, 335-341.
33. Y. Zhou, J. F. Zhang and J. Yoon, *Chem. Rev.*, 2014, **114**, 5511-5571.
34. G. Maroulis, C. Makris, D. Xenides and P. Karamanis, *Mol. Phys.*, 2000, **98**, 481-491.

### Figure Captions

- Fig. 1 FTIR spectra of SNP, sensor **A**, sensor **B**, and their intermediate products
- Fig. 2 (a) Nitrogen adsorption–desorption isotherms and (b) Barrett–Joyner–Halenda (BJH) pore diameters of SNP, sensor **A**, and sensor **B**.
- Fig. 3 TGA results showing the thermogram of (a) sensor **A** and (b) sensor **B**, and their intermediate products.
- Fig. 4 Fluorescence spectra of (a) sensor **A** ( $16.7 \text{ mg ml}^{-1}$ ) and (b) sensor **B** ( $20.4 \text{ mg ml}^{-1}$ ) in the presence of different amounts of TBAF in DMSO.
- Fig. 5 UV-vis absorption spectral changes in (a) sensor **A** ( $16.7 \text{ mg ml}^{-1}$ ) and (b) sensor **B** ( $20.4 \text{ mg ml}^{-1}$ ) upon titration with TBAF (0.0 to 1.5 mole equiv.) in DMSO.
- Fig. 6 (a) Fluorescence intensity increment  $[F-F_0]$  in sensor **A** [(A)  $50.0 \text{ mg ml}^{-1}$ , (B)  $100.0 \text{ mg ml}^{-1}$ , and (C)  $150.0 \text{ mg ml}^{-1}$ ] and sensor **B** [(D)  $61.2 \text{ mg ml}^{-1}$ , (E)  $122.4 \text{ mg ml}^{-1}$ , and (F)  $183.7 \text{ mg ml}^{-1}$ ] at  $542 \text{ nm}$  upon titration with  $150.0 \text{ mM}$ ,  $300.0 \text{ mM}$ , and  $450.0 \text{ mM F}^{-1}$  respectively. The insert shows the emission spectra for sensor **A** and sensor **B** at  $F^{-}$  : **FITC-OSMDBT** equiv. mole titration ratio of  $x : x$  ( $x = 3.0, 6.0, \text{ and } 9.0$ ). The spectra were recorded  $15.0 \text{ min}$  after addition of  $F^{-}$ . And (b) Plot of emission intensity ( $\lambda_{em} = 542 \text{ nm}$ ) versus TBAF concentration using values from A, B, and C.
- Fig. 7 (a) Fluorescence intensity increment  $[F-F_0]$  in sensor **A** [(A)  $33.0 \text{ mg ml}^{-1}$ , (B)  $66.1 \text{ mg ml}^{-1}$ , and (C)  $83.3 \text{ mg ml}^{-1}$ ] and sensor **B** [(D)  $40.8 \text{ mg ml}^{-1}$ , (E)  $81.6 \text{ mg ml}^{-1}$ , and (F)  $102.1 \text{ mg ml}^{-1}$ ] at  $542 \text{ nm}$  upon titration with  $100.0 \text{ mM}$ ,  $200.0 \text{ mM}$ , and  $250.0 \text{ mM F}^{-1}$  respectively. The spectra were recorded  $15 \text{ min}$  after addition of  $F^{-}$ . (b) Emission intensity increment ( $\lambda_{em} = 542 \text{ nm}$ ) in sensor **A** ( $16.7 \text{ mg ml}^{-1}$ ) and sensor **B** ( $20.4 \text{ mg ml}^{-1}$ ) at different times after addition of  $F^{-}$  ( $50.0 \text{ mM}$ ) in DMSO.

Fig. 8 (a) Selectivity of sensor **A** ( $16.7 \text{ mg ml}^{-1}$ ) and sensor **B** ( $20.4 \text{ mg ml}^{-1}$ ), and (b) sensor **A** ( $50.0 \text{ mg ml}^{-1}$ ) and sensor **B** ( $61.2 \text{ mg ml}^{-1}$ ) towards  $\text{F}^-$  over  $\text{Cl}^-$ ,  $\text{Br}^-$ ,  $\text{I}^-$ , and  $\text{NO}_3^-$  (at a concentration of 50 mM respectively) in DMSO.

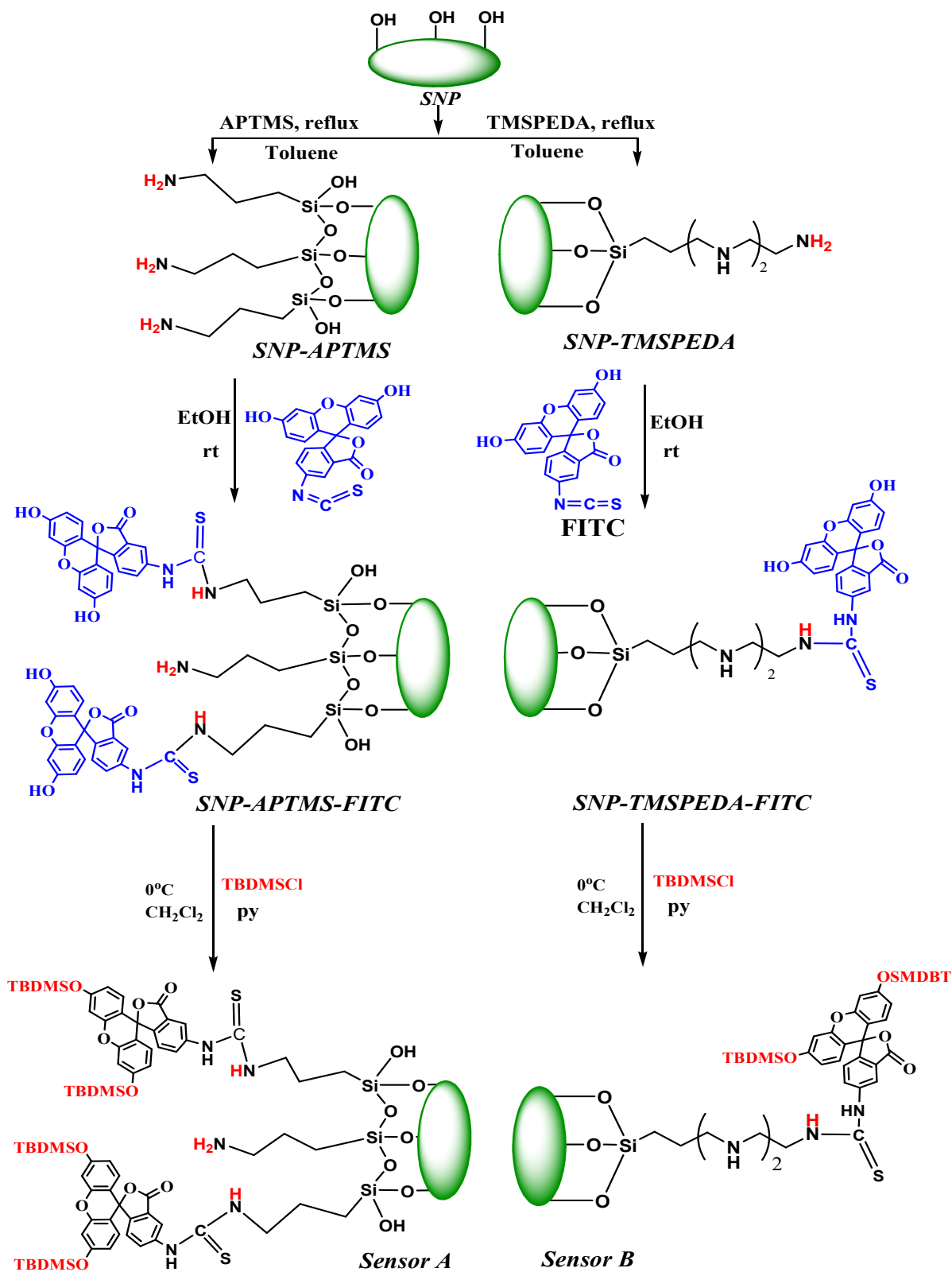
Fig. 9 Color change in sensor **B** ( $20.4 \text{ mg ml}^{-1}$ ) after the addition of 50.0 mM tetrabutylammonium salts (from left to right:  $\text{Cl}^-$ ,  $\text{I}^-$ ,  $\text{Br}^-$ ,  $\text{NO}_3^-$ , and  $\text{F}^-$ ).

### Scheme captions

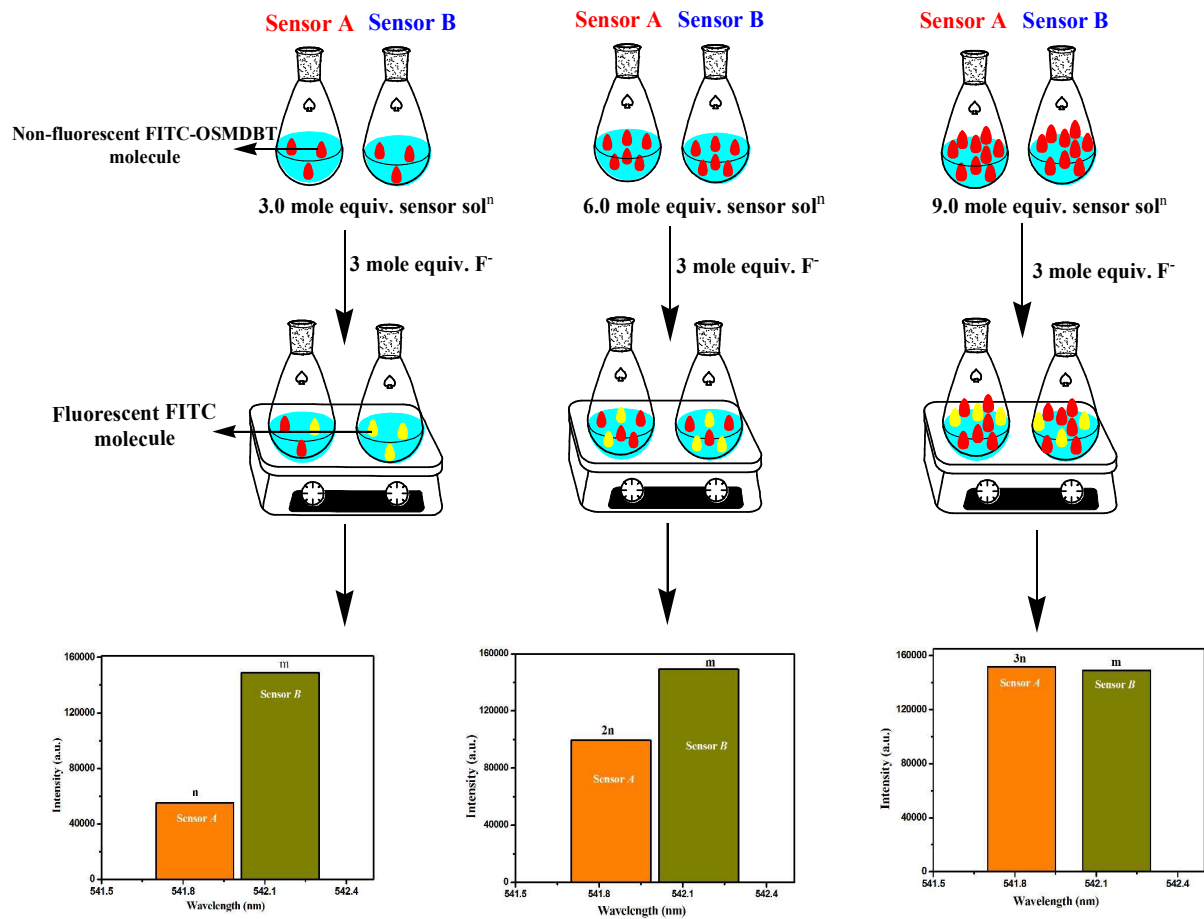
Scheme 1 Synthesis route to sensor **A** and sensor **B**.

Scheme 2 Schematic illustrations of the titration of 3.0 mole equiv.  $\text{F}^-$  against sensor solutions containing 3.0, 6.0, and 9.0 mole equiv. SFITC molecules. The insert shows their emission intensity values measured at 542nm.





Scheme 1



Scheme 2

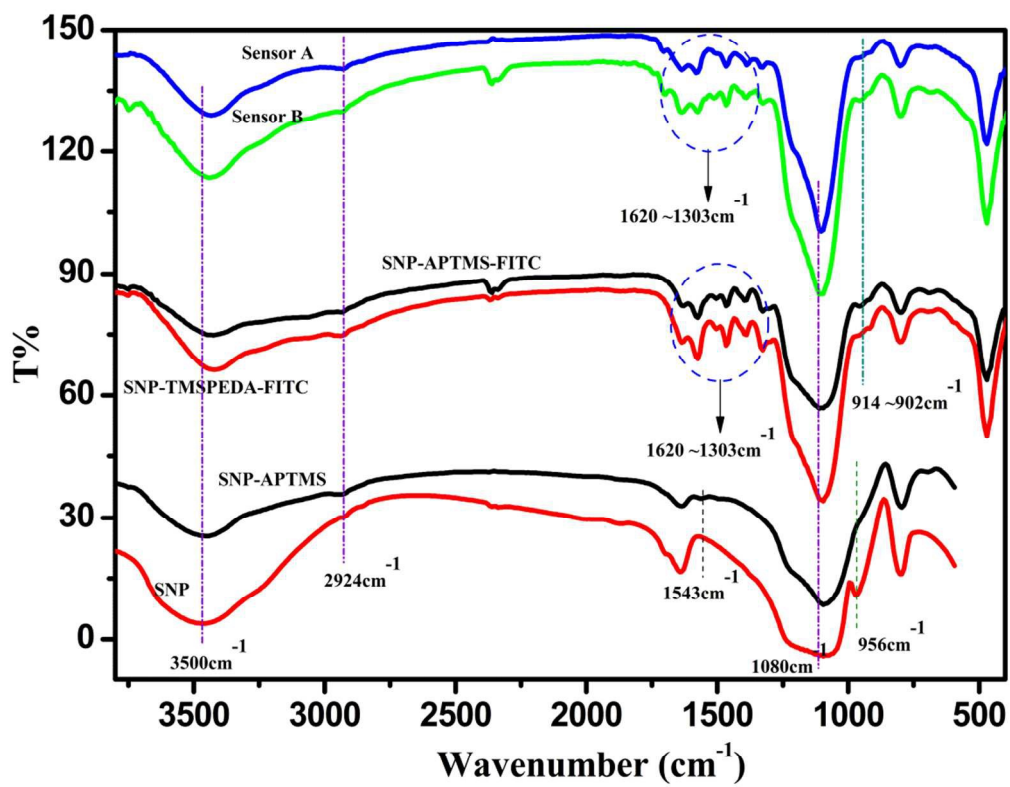
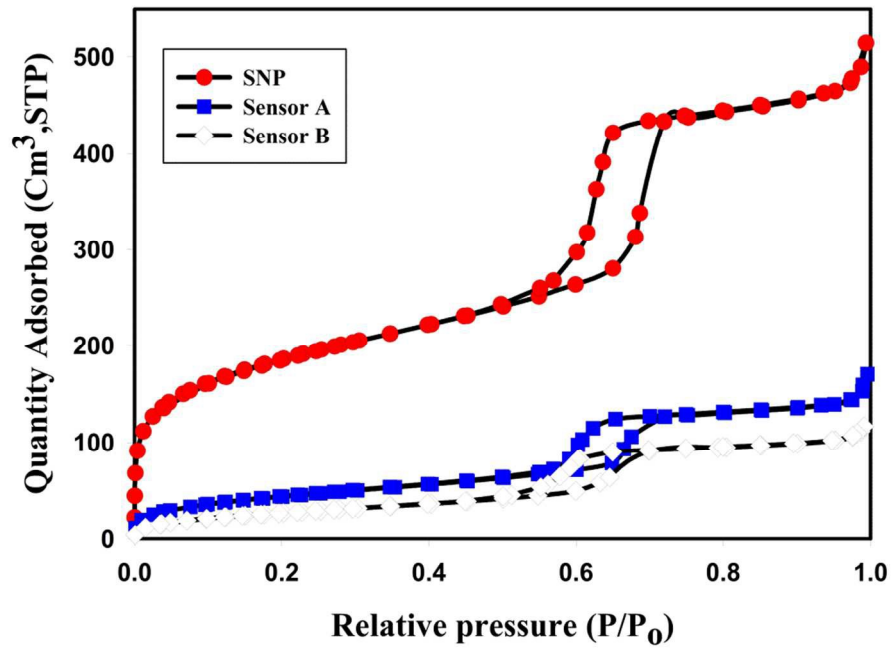
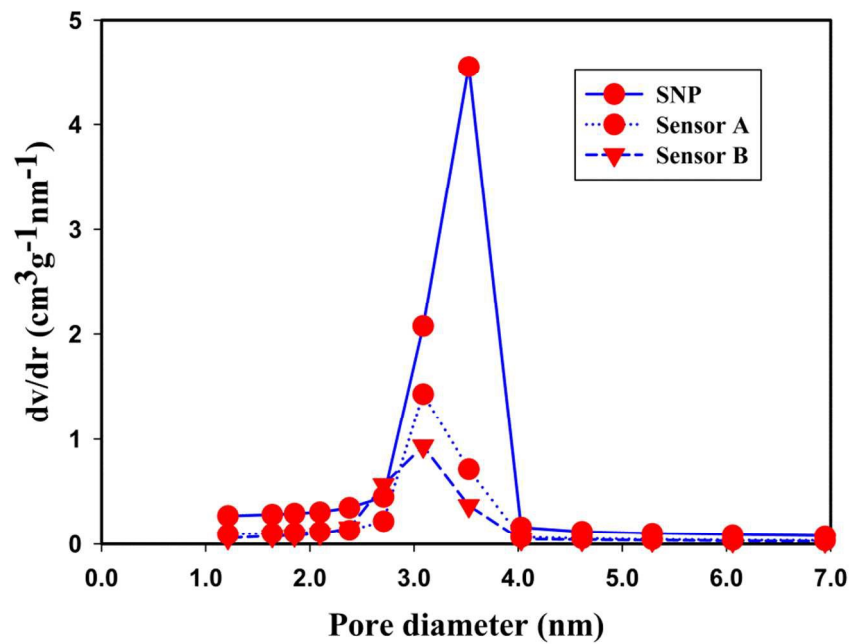


Fig. 1

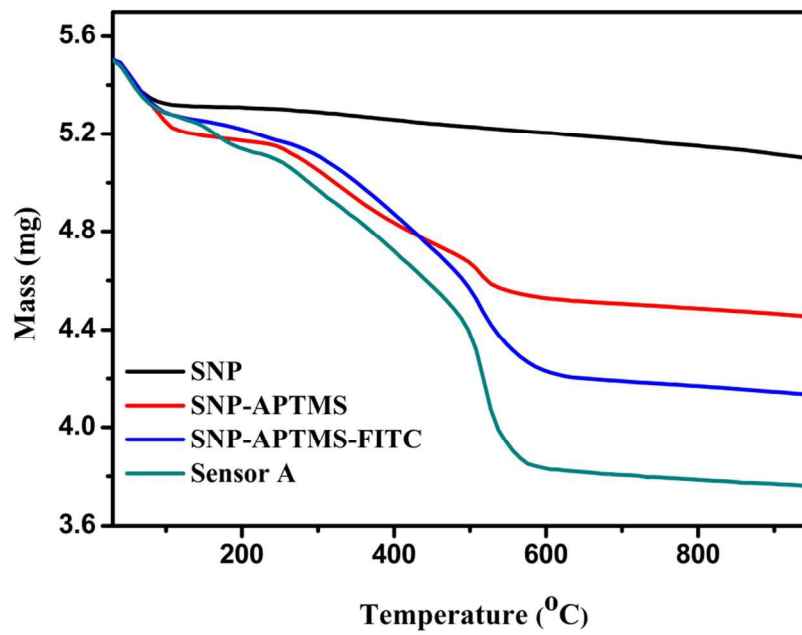


(a)

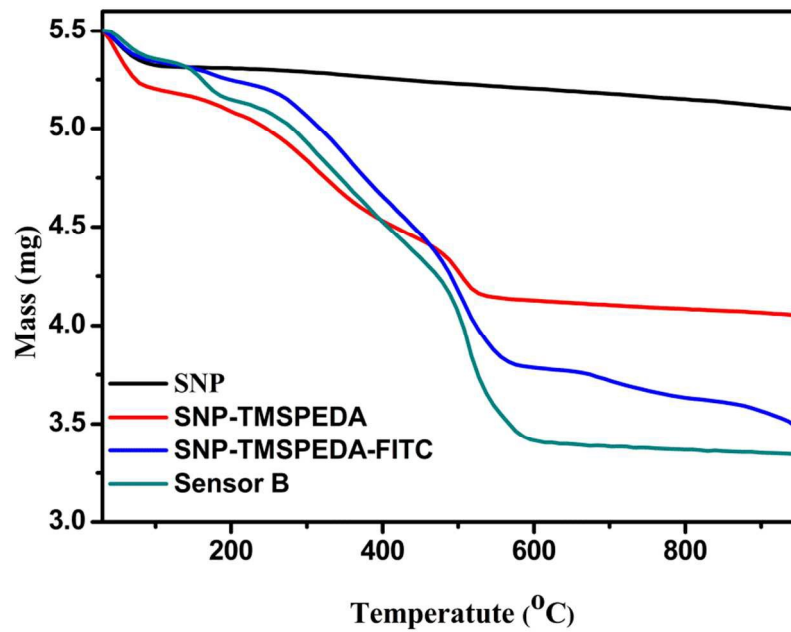


(b)

Fig. 2

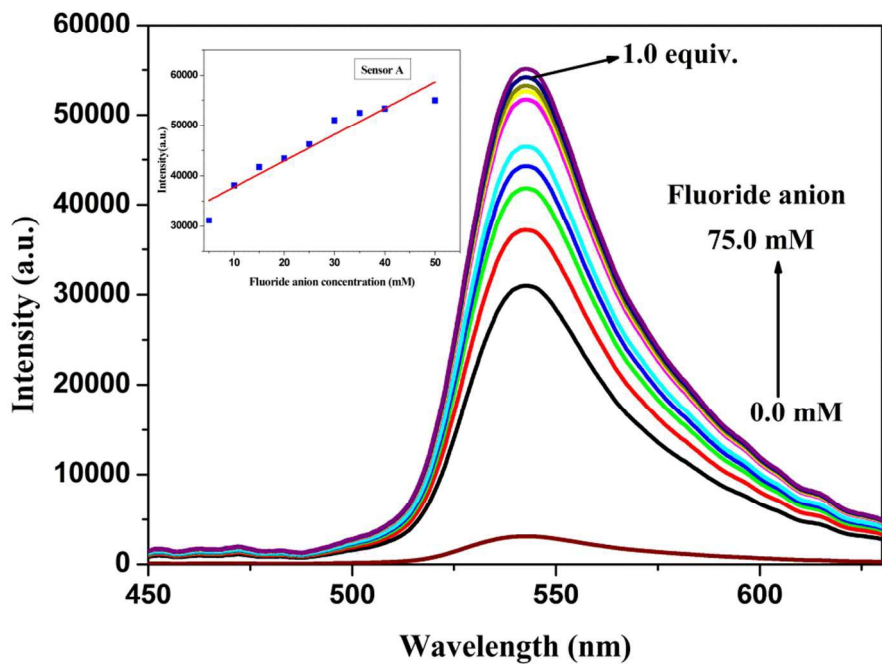


(a)

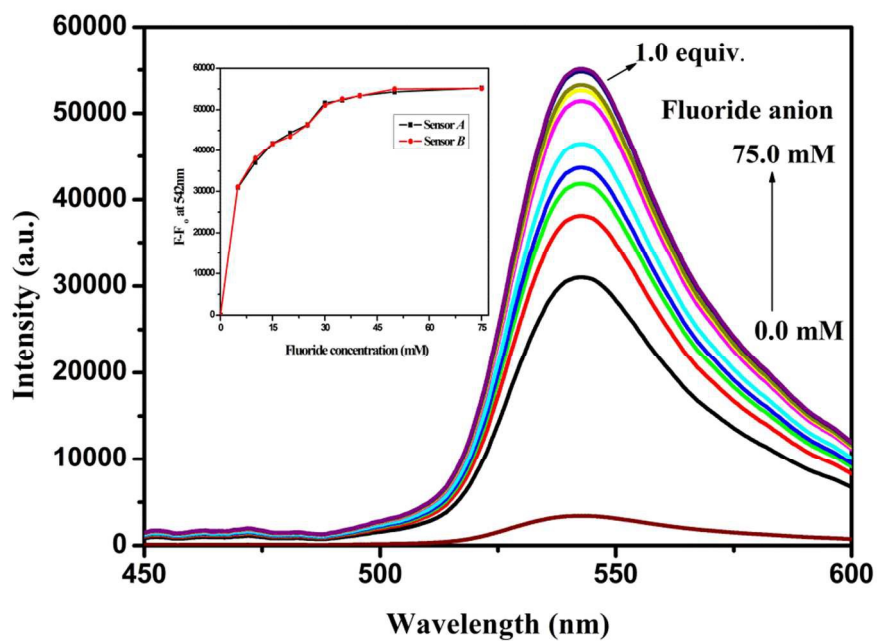


(b)

Fig. 3

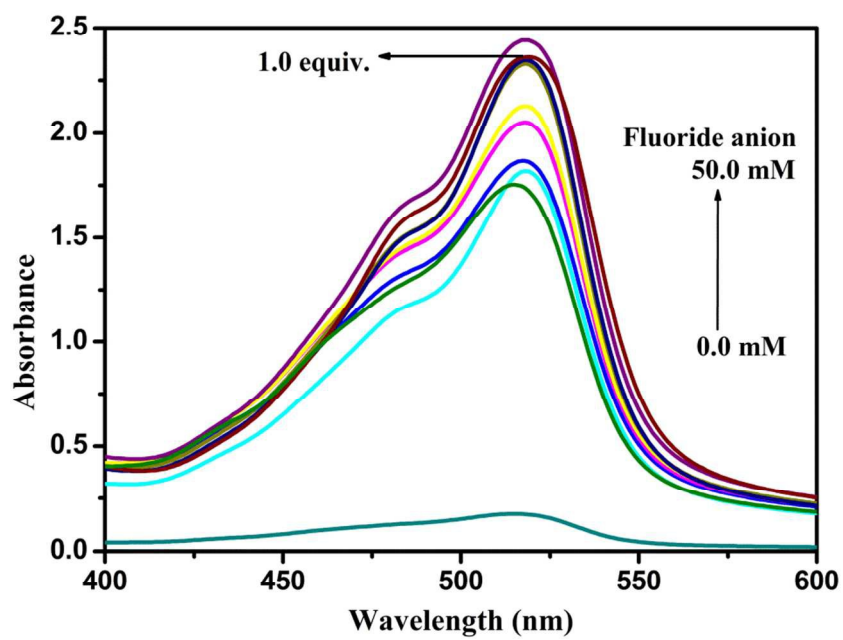


(a)

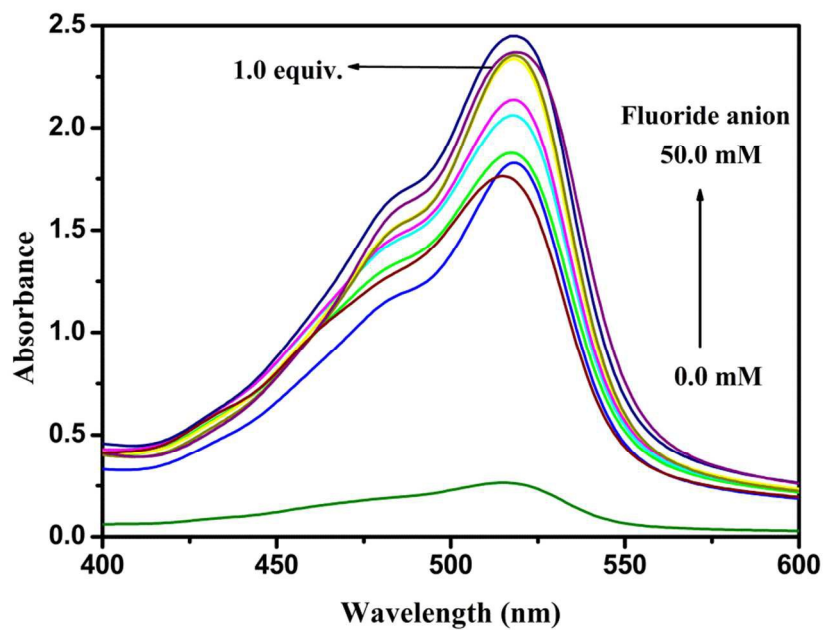


(b)

Fig. 4

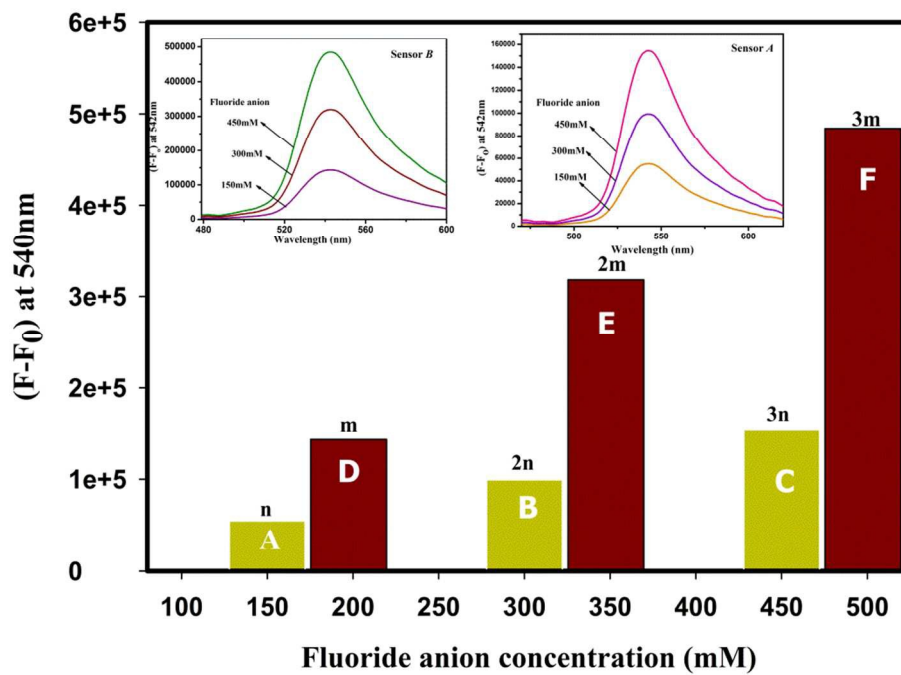


(a)

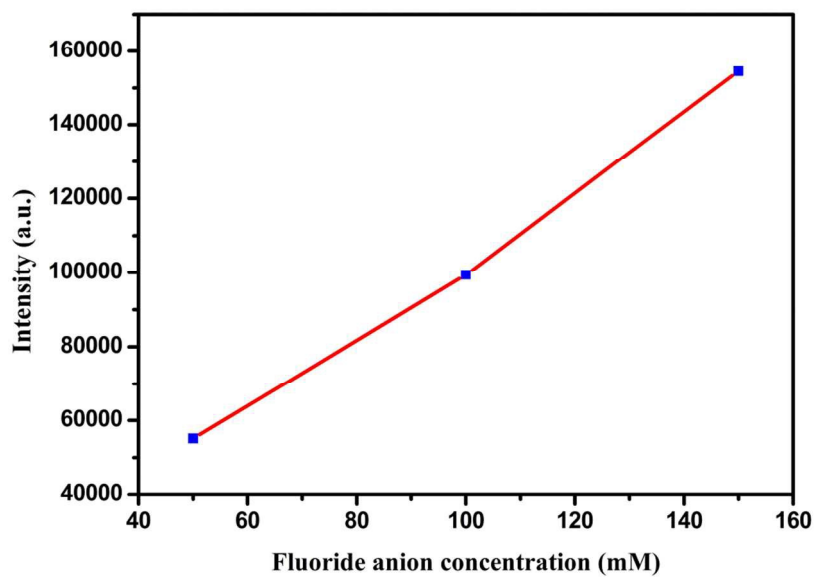


(b)

Fig. 5



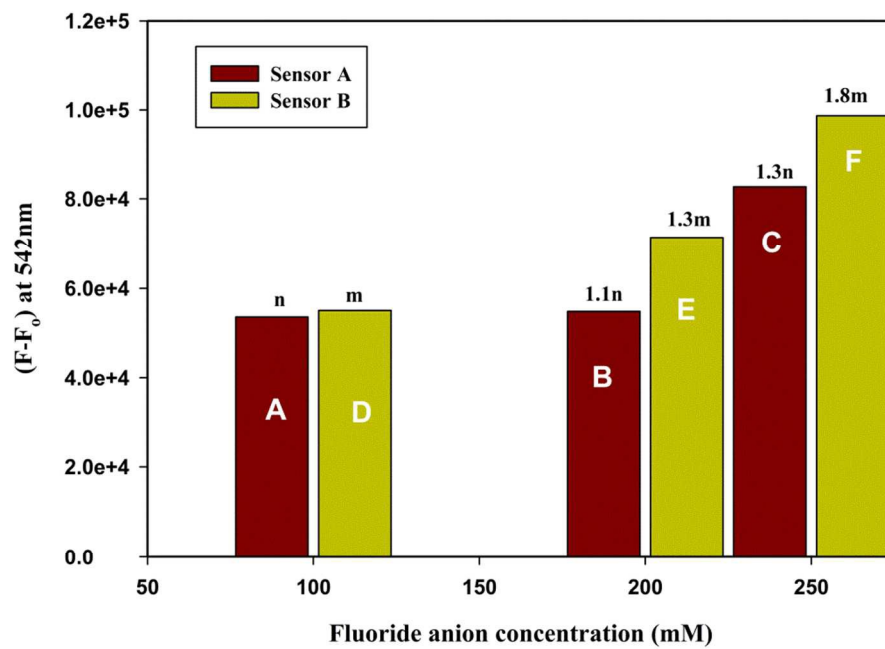
(a)



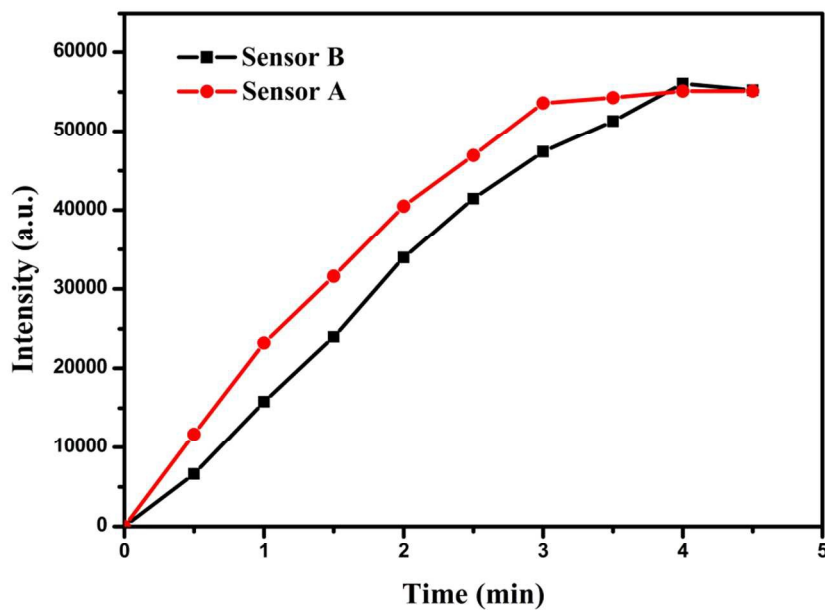
(b)

Fig. 6



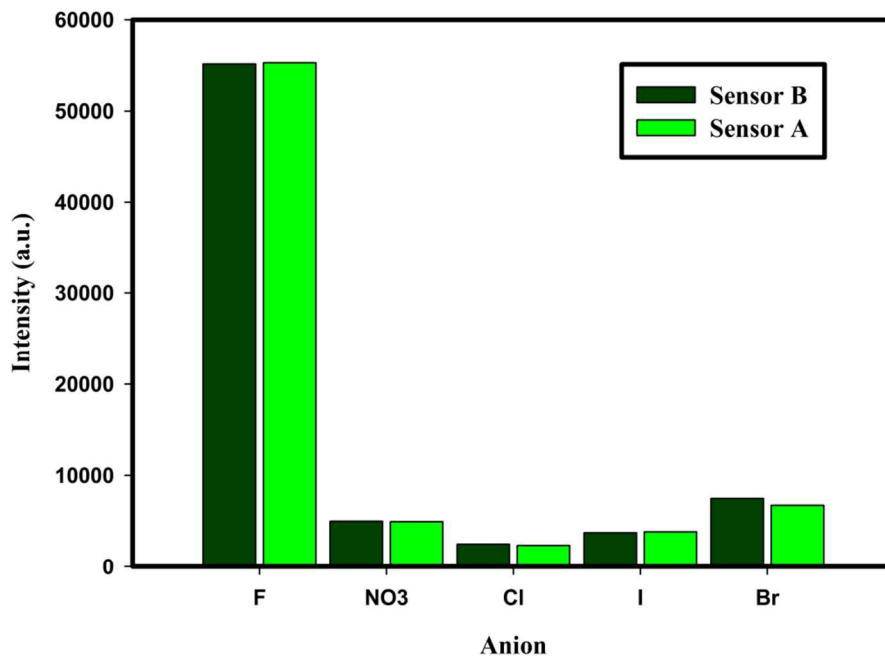


(a)

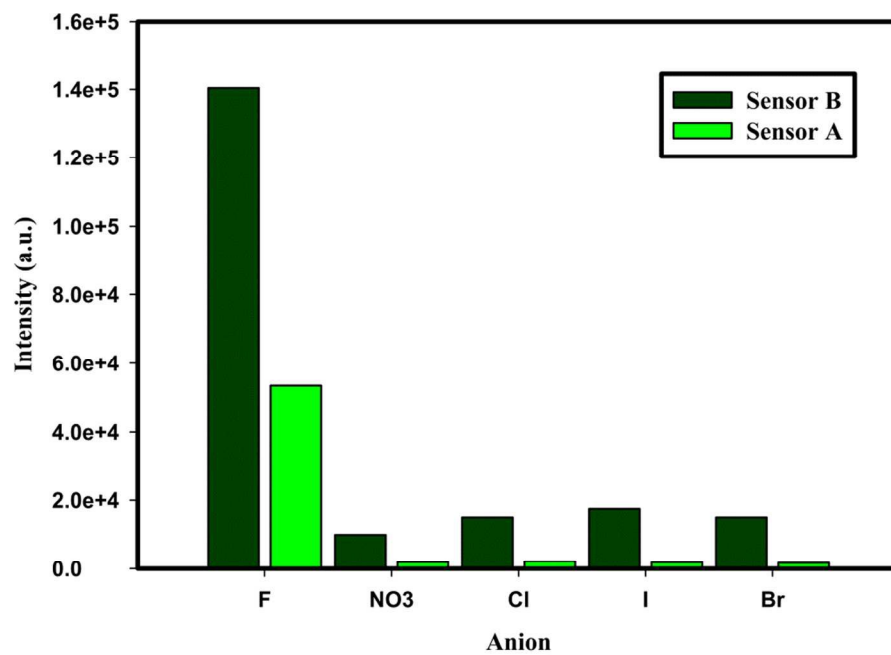


(b)

Fig. 7

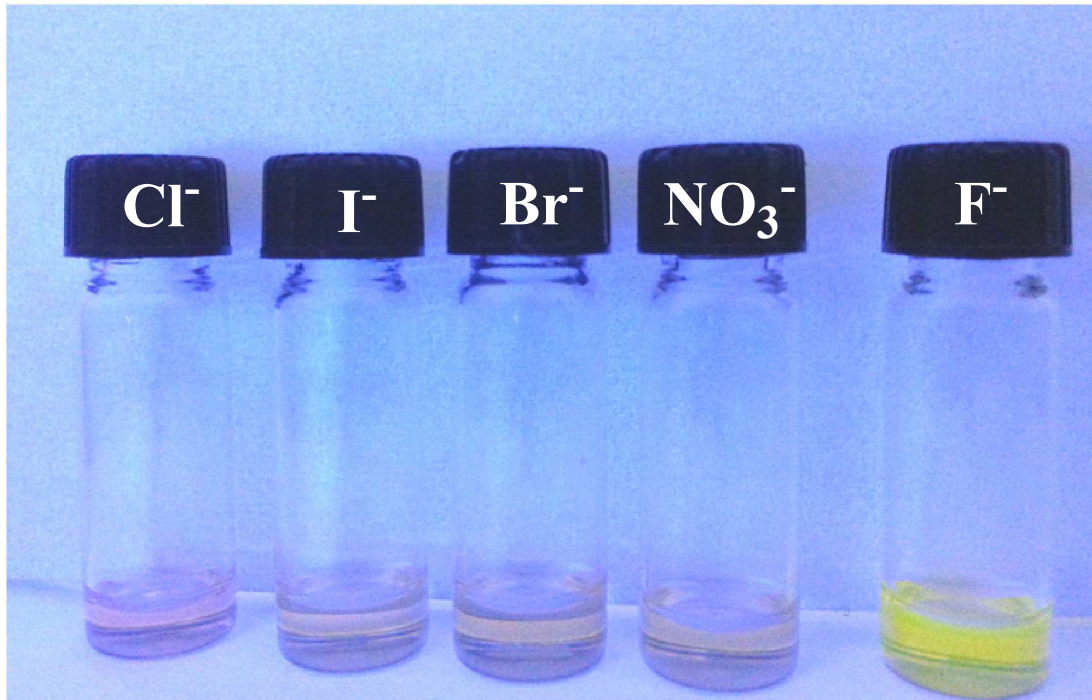


(a)



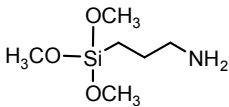
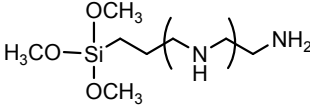
(b)

Fig. 8



**Fig. 9**

**Table 1** Chemical structure of the alkoxysilane molecules used to modify the surface of SNP

Chemical name	Designation	Chemical structure
3-aminopropyltrimethoxysilane	APTMS	
N-[3-(Trimethoxysilyl)propyl]ethylenediamine	TMSPEDA	

**Table 2** EDX for SNP, sensor *A*, and sensor *B*

sample	Weight %				Atomic%			
	Carbon	Oxygen	Silicon	Sulfur	Carbon	Oxygen	Silicon	Sulfur
SNP	-	69.08	30.92	-	-	79.68	20.32	-
Sensor <i>A</i>	33.7	48.91	17.05	0.32	43.31	47.17	9.37	0.15
Sensor <i>B</i>	51.90	40.94	6.93	0.23	60.57	35.87	3.46	0.10

**Table 3** Barrett–Joyner–Halenda pore diameter ( $d_{\text{BJH}}$ ), Brunauer–Emmett–Teller surface area ( $S_{\text{BET}}$ ), and pore volume ( $V_{\text{p}}$ ) of SNP, sensor *A*, and sensor *B*

Material	$d_{\text{BJH}}$ (nm)	$S_{\text{BET}}$ ( $\text{m}^2\text{g}^{-1}$ )	$V_{\text{p}}$ ( $\text{cm}^3\text{g}^{-1}$ )
SNP	4.58	674.65	0.77
Sensor <i>A</i>	5.97	161.05	0.24
Sensor <i>B</i>	7.19	98.81	0.18

**Table 4** TGA results of the number of moieties loaded on sensor **A** and sensor **B** and their intermediate products

Material	Moiety (X)	Reaction step	X (mmol/g)	(X nm <sup>-2</sup> ) <sup>a</sup>
SNP	OH	-	2.40	2.14
SNP-APTMS	APTMS	Silanization	0.82	0.73
SNP-TMSPEDA	TMSPEDA		1.33	1.18
SNP-APTMS- FITC	FITC	FITC immobilization	0.84	0.75
SNP-TMSPEDA- FITC	FITC	FITC immobilization	0.58	0.52
Sensor <b>A</b>	TBDMSCI	Silylation	0.66	0.60
Sensor <b>B</b>			0.49	0.40

<sup>a</sup>Based on the SNP surface area of 674.65 m<sup>2</sup>g<sup>-1</sup>.

**Table 5** Performance of sensor *A* vs. sensor *B*

Sensor	Detection range <sup>a</sup> (mM)	Selectivity <sup>b</sup>
<i>A</i>	0.0 ~ 50.0	53784.0 a.u.
<i>B</i>	0.0 ~150.0	140943.0 a.u.
% difference	-	162.0

<sup>a</sup> Based on a fluoride ion : FITC-OSMDBT equiv. mole titration ratio of 3.0 : 3.0

<sup>b</sup> Based on intensity values from Fig. 7b: 53784 a.u. was used as the basis for calculation.